Applied Physics Letters ARTICLE pubs.aip.org/aip/apl

Deep learning-assisted local resonance strategy for accurate internal damage imaging in composites

Cite as: Appl. Phys. Lett. **125**, 194102 (2024); doi: 10.1063/5.0233476
Submitted: 14 August 2024 · Accepted: 22 October 2024 ·
Published Online: 4 November 2024

Changyu Zhang,[1] Yajie Hu,[1] Mingxi Deng,[2,a)] and Weibin Li[1,a)]

AFFILIATIONS

[1]School of Aerospace Engineering, Xiamen University, Xiamen 361005, China
[2]College of Aerospace Engineering, Chongqing University, Chongqing 400044, China

[a)]Authors to whom correspondence should be addressed: mxdeng@cqu.edu.cn and liweibin@xmu.edu.cn

ABSTRACT

In this paper, we propose a deep neural network-assisted strategy to accurately and efficiently identify local defect resonance (LDR) modes and accurately image the internal damage in composites. A two-dimensional convolutional neural network (2D-CNN) model was constructed to identify LDR modes. The frequency-domain contour maps were used as input data, given that the LDR phenomenon exhibits discernible physical attributes in the frequency domain that are conducive to deep neural network assimilation. The obtained results demonstrate effective training outcomes and transferability, even with a limited number of samples. The LDR modes are efficiently extracted by the developed 2D-CNN model and used to obtain the accurate imaging of internal damages in composites.

The resonant phenomenon is a fascinating topic in elastic acoustic wave research. Over the past decades, numerous studies on local resonance, such as acoustic metamaterials[1,2] and non-propagating modes,[3,4] have garnered significant attention. In particular, the internal defect-induced local energy trapping effect, known as local defect resonance (LDR), has become noteworthy due to its great potential in non-destructive evaluation.[5–10] Researches revealed that the physical mechanism of LDR is the resonance of the transmitting and reflecting guided waves in the damage area.[11–14] These investigations enable the prediction of both first-order and higher-order LDR frequencies and demonstrate a close relationship between LDR frequencies and damage size. Certainly, the primary appeal of LDR lies in its high efficiency for damage imaging in complex materials or structures, such as composites. LDR can directly indicate the location of damage without complex algorithmic procedures, yet it achieves a high signal-to-noise ratio (SNR).[15–17] Various damage imaging methods, such as wideband spectrum analysis[18] and multi-mode integration,[19] have been developed to quantitatively evaluate local flat bottom holes,[20,21] delamination,[22,23] and impact damages[24,25] in composites using laser scanning Doppler vibrometer (LSDV) and thermal imagery-based techniques.

The use of LDR-based damage imaging technique has been proven as a promising alternative for internal damages identification in composites.[22,23] However, the accurate determination of LDR frequencies is still challenging, which limits the effectiveness of the approach for the precise assessment of internal damage. To address this limitation, various methods have been reported, including the damage-background ratio (DBR),[26] weighted band power (WBP),[7] and nonlinear narrow sweep excitation (NNSE).[27] These methods, however, rely on one-dimensional spectral analysis and require domain expertise and prior knowledge of LDR. Although physical mechanism-based formulas can theoretically calculate LDR frequencies, they are only applicable to simple, approximately two-dimensional isotropic waveguide structures. These challenges in acquiring resonance frequencies significantly limit the practical application of LDR-based techniques.

Deep neural networks (DNN) have garnered attention due to their success in efficiently learning features from raw signals, becoming the dominant approach for image analysis and mechanical system diagnosis.[28–30] Notably, the LDR phenomenon exhibits discernible physical attributes in the frequency domain, which are considerably conducive to deep neural network assimilation. However, despite the great potential of deep learning-assisted LDR method, investigations on combining DNN with the LDR effect are still lacking. In this paper, we introduce a deep learning-assisted strategy to overcome the difficulties in identifying LDR modes. The proposed method is to determine the LDR frequencies with improved accuracy and efficiency, for accurate imaging of internal damages in composites.

Specifically, the flow chart of this strategy is shown in Fig. 1. In this study, the time-domain vibration fields (TDVFs) of a damaged

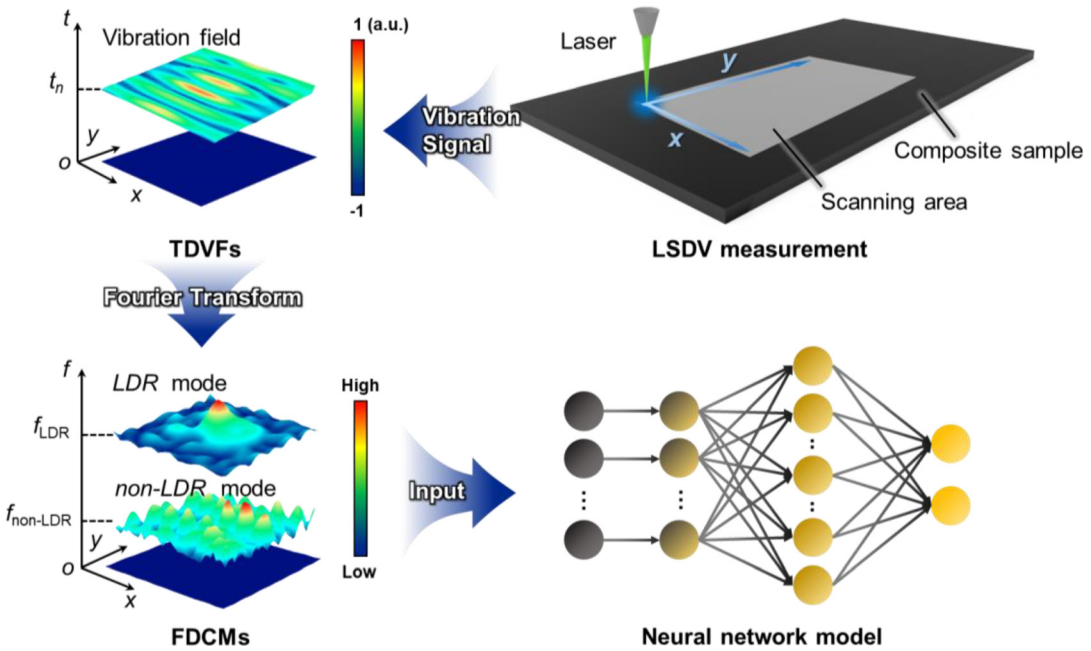

FIG. 1. Schematic of the flow chart of the deep learning assisted LDR identification and internal damage imaging strategy.

composite plate were measured using the LSDV system. Subsequently, one-dimensional fast Fourier transformation (1DFFT) was applied to obtain frequency-domain contour maps (FDCMs). Thousands of FDCMs were manually pre-labeled as *LDR* and non-*LDR* and used to train the neural network. The input FDCMs contain the information of both frequency-domain vibration fields and the corresponding frequencies. Thus, the well-trained neural network can identify the LDR modes and determine the LDR frequencies of various types of damage and further assist in accurately imaging the internal damages.

The test specimen is a [90°/0°/90°/0°] symmetrically layered T300/M914 carbon fiber reinforced polymer (CFRP). Given that the mechanical properties are critical for identifying LDR modes, the specific material parameters are presented in Table I. Here, 90° indicates that the fibers are oriented in the *x*-direction. The specimen dimensions are $300 \times 300 \times 1.5\,\text{mm}^3$. Two different shapes of internal damage—circular and triangular, each with a thickness of 0.1 mm—were artificially introduced into the first and second plies. The internal damages were induced by inserting two layers of 0.05 mm thickness brass foil, and the manufacturing process is depicted in Fig. 2(b). The two edges of brass foil were bonded together to effectively create delamination within the specimen.[19] In this work, the LDR effect of delamination in composites was induced using these setups.

The experimental setup is illustrated in Fig. 2(a). To measure the vibration signals in the specimens, a LSDV system (Polytec PSV-500) was applied. The 1–50 kHz bandwidth chirp signal was generated from the Polytec signal generator and acts on the $15 \times 1\,\text{mm}^2$ piezoelectric transducer (PZT) to generate the guided waves into the specimens. A high-performance power amplifier (KH-7600M) was

TABLE I. Density (kg/m^3) and stiffness parameters (GPa) of the T300/M914 composite.

ρ	C_{11}	C_{12}	C_{13}	C_{23}	C_{22}	C_{33}	C_{44}	C_{55}	C_{66}
1493	135.4	7.40	7.40	9.51	2.9	9.51	3.31	3.89	3.89

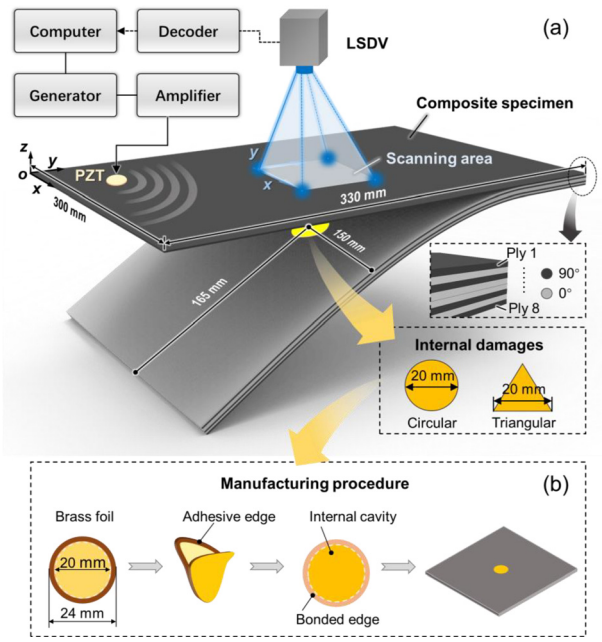

FIG. 2. Schematic of experimental settings: (a) the LSDV system and composite specimen and (b) the manufacturing procedure of the damages.

employed to provide sufficient excitation voltage. The sampling rate was set to 200 kHz, with a special sampling interval of 1.0 mm to ensure adequate analytical resolution.

In this paper, a two-dimensional convolutional neural network (2D-CNN) model was developed for identifying LDR modes. To train the neural network model, we recorded the vibration fields of composite specimens with circular damage. Considering the TDVFs $s_\Omega(t)$ alone do not fully capture the characteristics of LDR phenomenon, we transformed the TDVFs into FDCMs $A_\Omega(f)$ using the 1DFFT,

$$A_\Omega(f) = \left|F_{1D}[s_\Omega(t)]\right|, \tag{1}$$

where Ω is the scanning area and f represents the frequency. The transformed FDCMs contain LDR and non-LDR features and are used as the input for training and testing the 2D-CNN model.

As shown in Fig. 3, the 2D-CNN model is constructed with convolutional, max pooling, and fully connected layers. The max pooling module is applied to reduce the size of the dataset during training by extracting and retaining the maximum feature value from the pooling process. The hidden layers include multiple convolutional and max pooling operations. The convolutional filters are set to a size of 3×3, and the ReLU activation function is used. The mathematical formula for the 2D convolution can be expressed as

$$X_\xi^l = \sum_{\zeta=1}^{N_{l-1}} conv2D\left(W_{\zeta\xi}^l, X_\zeta^{l-1}\right) + B_\xi^l, \tag{2}$$

$$Y_\xi^l = \mathcal{F}\left(X_\xi^l\right), \tag{3}$$

where X_ξ^l is the output of the ξth neuron at lth layer, $W_{\zeta\xi}^l$ is the weight of the ζth neuron at l-1th layer to the ξth neuron at lth layer, X_ζ^{l-1} is the output of ζth neuron at l-1th layer, B_ξ^l is the bias of ξth neuron at lth layer, $conv2D(,)$ is the 2D convoluation, and Y_ξ^l is the output through the activation function $\mathcal{F}(\cdot)$. Thereafter, the fully connected layer consolidates the feature values and output the results as "0" and "1", where "0" denotes non-LDR modes and "1" denotes the LDR modes.

The proportion of LDR modes can affect the accuracy of the identification results. Specifically, compared to a low proportion, the use of high proportion of LDR modes tends to achieve more accurately results. However, a low proportion of LDR modes is the general case in practical investigation. Thus, during the CNN model training, the gradient descent method (GTM) was employed to optimize the parameters W and B within the neural network architecture, enhancing its accuracy in identifying LDR modes, even at lower proportion. The frequency-domain contour maps (FDCMs) of specimens with circular damage were used for training the CNN model. These FDCMs were pre-analyzed and labeled as *LDR* and non-*LDR* modes. The proportion of *LDR* modes was varied from 50% to 5%, with a total of 3465 FDCMs used at the 5% *LDR* modes. The data were split into training and testing sets in 8:2 ratio. For example, in the case of 5% *LDR* modes, 80% of the 3465 FDCMs were used for training, and 20% were used for testing. Figures 4(a) and 4(b) show the confusion matrices for cases with 130 FDCMs (25% *LDR* modes) and 693 FDCMs (5% *LDR* modes) used for testing, respectively. The accuracies achieved were 97.69% and 99.71%, indicating that the 2D-CNN model was effectively trained using the GTM.

Figures 4(d) and 4(f) show normalized FDCMs of the identified non-*LDR* and *LDR* modes, respectively. In contrast to the non-*LDR* modes, the *LDR* modes exhibit a strong local energy trapping effect at the damage area, clearly indicating the location of the internal damage with high SNR. For comparison, the DBR method was also applied to calculate the LDR frequencies, which can be expressed as follows:

$$DBR(f) = \frac{MAX[A_\Omega(f)]}{MEAN[A_\Omega(f)]}. \tag{4}$$

Here, a threshold of more than 10 times the $MAX[A_\Omega(f)]$ to the $MEAN[A_\Omega(f)]$ was used to recognize high-SNR local resonance vibrations. As shown in Fig. 4(c), three prominent peaks in the DBR spectrum correspond to LDR frequencies of 9.01, 9.83, and 17.75 kHz. These LDR frequencies align well with those identified by the 2D-CNN model. Notably, in addition to these frequencies, the well-trained 2D-CNN model also identified other *LDR* modes at 8.17 and 13.42 kHz, which are difficult to detect using the DBR method.

Furthermore, an internal damage imaging approach was implemented by integrating the *LDR* modes identified by the 2D-CNN. The integration method can be expressed as follows:[18]

$$I_\Omega = \sum_{i=1}^{n} q_i A_\Omega^{LDR_i}, \tag{5}$$

$$q_i = \frac{\iint_\Omega A_\Omega^{LDR_i} d\Omega}{\sum_{j=1}^{n} \iint_\Omega A_\Omega^{LDR_j} d\Omega}, \tag{6}$$

where I_Ω refers to the integrated vibration field of the scanning area Ω, q_i represents the weighting parameter, and $A_\Omega^{LDR_i}$ is the FDCMs of the

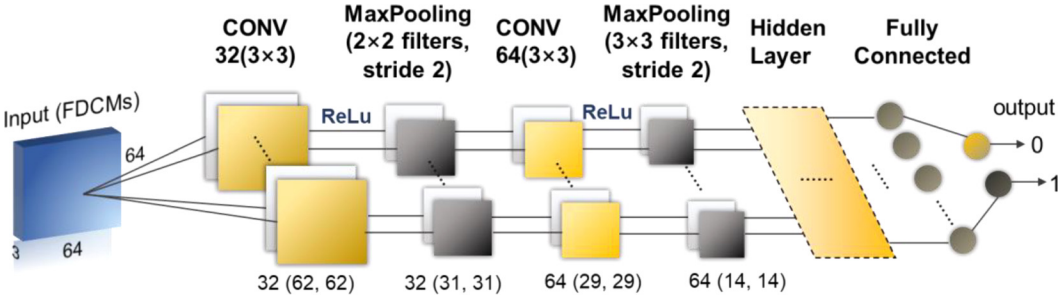

FIG. 3. The specific structure of the 2D-CNN model.

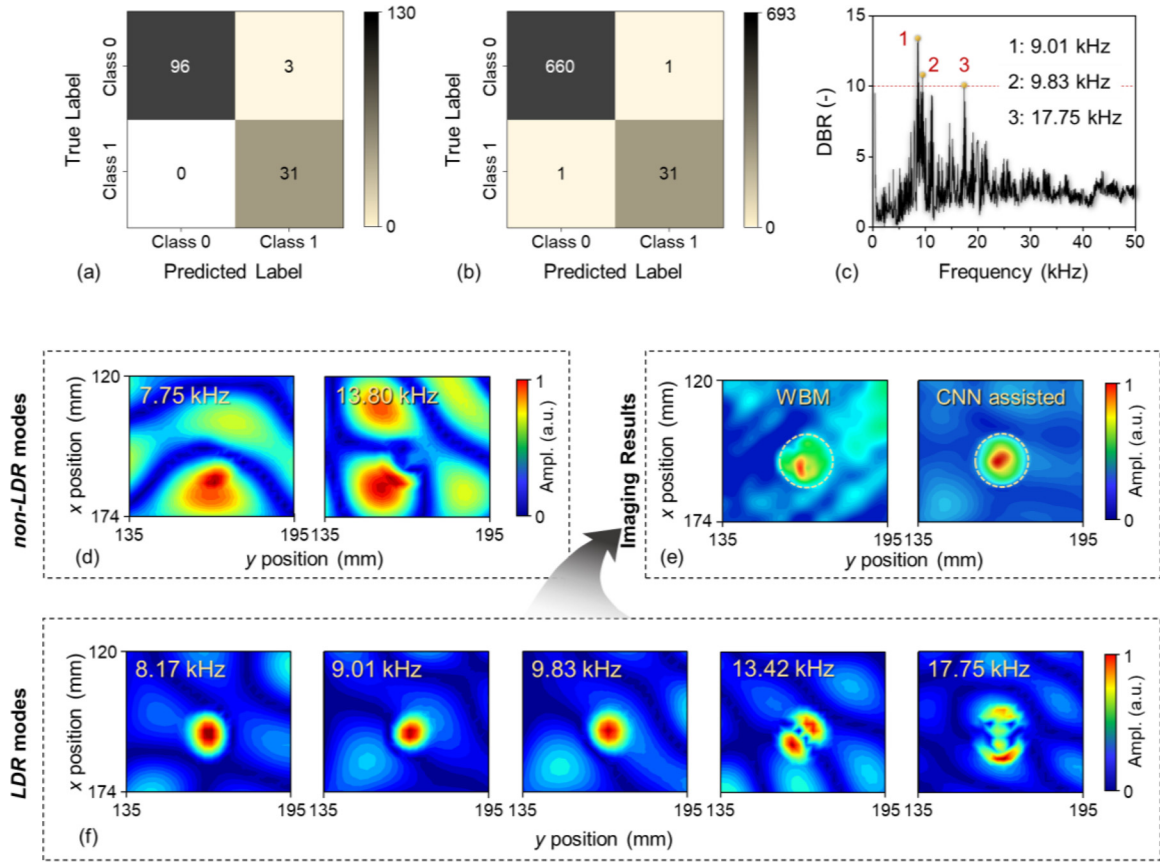

FIG. 4. The training results of the 2D-CNN model. The confusion matrixes calculated in the case of (a) 130 FDCMs (25% *LDR* modes) and (b) 693 FDCMs (5% *LDR* modes) for testing, respectively. (c) The DBR spectrum of for LDR frequency identification. (d) The non-*LDR* and (f) *LDR* modes identified by the 2D-CNN model. (e) The imaging results of the circular damage using 1–50 kHz WBM and CNN assisted (the dash line indicates the actual damage profile).

scanning area Ω at the *i*th-order LDR frequency. The normalized imaging results are shown in Fig. 4(e), where the dashed line represents the actual profile of the manufactured circular damage. For comparison, the LDR-based wideband method (WBM) was also applied for damage imaging. Both imaging results shown in Fig. 4(e) closely match the actual internal damage. However, in contrast to the WBM results, the CNN assisted imaging exhibits higher SNR and more precisely visualizes the size and location of the circular damage. These findings convincingly demonstrate the significant advantages of this deep learning assisted strategy for internal local damage imaging.

Further procedures were implemented to verify the transferability of the proposed deep learning assisted strategy in addressing different types of damage. The triangular damage was chosen as a more complex case, given the significant differences between triangular and circular damage (e.g., sharper corners and smaller size). Figure 5(a) illustrates the normalized FDCMs of the identified first- and second-order *LDR*

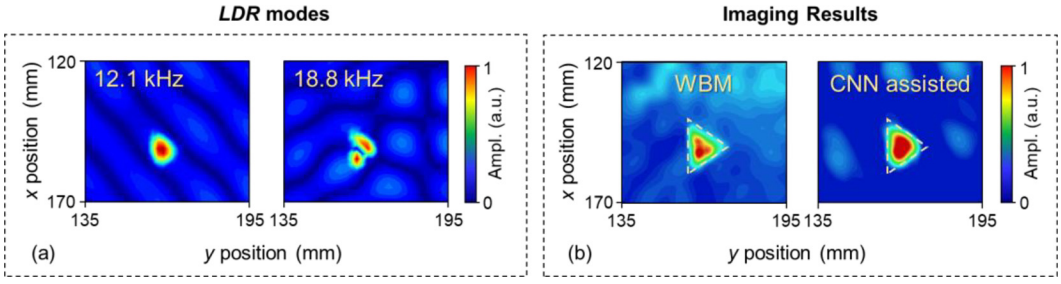

FIG. 5. (a) Identified *LDR* modes at 12.1 and 18.8 kHz of the triangular damage. (b) The imaging results of the triangular damage using 1–50 kHz WBM and CNN assisted (the dash line indicates the actual damage profile).

modes of the triangular damage. Figure 5(b) shows the imaging result using the 1–50 kHz WBM and deep learning assisted strategy, with the dashed line representing the actual profile of the manufactured triangular damage. The results in Fig. 5(b) demonstrate that the proposed CNN assisted imaging clearly captures the profile and size of the triangular damage with higher SNR. These findings prove that the proposed deep learning assisted strategy has a comparable capability to image the profile and size of more complex damage with a higher SNR.

The results in this paper demonstrate that precise imaging of different internal defects in composites with high-efficiency identification of LDR modes, can be achieved through the deep learning assisted strategy. This strategy overcomes the disadvantages of traditional methods, which require prior knowledge of LDR and are prone to misidentifying LDR frequencies. Additionally, the well-trained 2D-CNN model was effectively used to identify LDR modes in a triangular damage case, evidencing its robust capability to generalize and transfer across different types of damage and specimen configurations. Thus, the introduction of this method is of significance in overcoming the existing limitations in the application of LDR-based approaches.

This work was supported by the National Natural Science Foundation of China (Grants Nos. 12134002, 11974295, and 12074050). It also supported by the project of Natural Science Foundation of Fujian Province of China (Grant No. 2022J06007).

AUTHOR DECLARATIONS

Conflict of Interest

The authors have no conflicts to disclose.

Author Contributions

Changyu Zhang: Data curation (equal); Formal analysis (equal); Investigation (equal); Methodology (equal); Software (equal); Validation (equal); Writing – original draft (equal). **Yajie Hu:** Conceptualization (supporting); Data curation (equal); Formal analysis (equal); Investigation (supporting); Methodology (supporting); Software (equal); Validation (equal). **Mingxi Deng:** Conceptualization (equal); Funding acquisition (equal); Methodology (equal); Project administration (equal); Supervision (equal); Validation (equal); Writing – original draft (equal). **Weibin Li:** Conceptualization (equal); Formal analysis (equal); Funding acquisition (equal); Investigation (equal); Project administration (equal); Resources (equal); Supervision (equal); Validation (equal); Writing – original draft (equal).

DATA AVAILABILITY

The data that support the findings of this study are available within the article.

REFERENCES

[1]G. Liao, C. Luan, Z. Wang, J. Liu, X. Yao, and J. Fu, "Acoustic metamaterials: A review of theories, structures, fabrication approaches, and applications," Adv. Mater. Technol. **6**(5), 2000787 (2021).
[2]G. Ma, M. Yang, S. Xiao, Z. Yang, and P. Sheng, "Acoustic metasurface with hybrid resonances," Nat. Mater. **13**(9), 873–878 (2014).
[3]R. E. Morales, N. Pathak, J. S. Lum, C. M. Kube, T. W. Murray, and D. M. Stobbe, "Acoustoelastic characterization of plates using zero group velocity Lamb modes," Appl. Phys. Lett. **124**(8), 084101 (2024).
[4]C. Zhang, W. Li, and M. Deng, "Experimental observation of zero-group velocity combined harmonic generated by counter-directional Lamb wave mixing," Ultrasonics **143**, 107413 (2024).
[5]L. H. Tenek, E. G. Henneke, and M. D. Gunzburger, "Vibration of delaminated composite plates and some applications to non-destructive testing," Compos. Struct. **23**(3), 253–262 (1993).
[6]I. Solodov and M. Kreutzbruck, "Mode matching to enhance nonlinear response of local defect resonance," J. Sound Vib. **461**, 114916 (2019).
[7]J. Segers, S. Hedayatrasa, E. Verboven, G. Poelman, W. Van Paepegem, and M. Kersemans, "Efficient automated extraction of local defect resonance parameters in fiber reinforced polymers using data compression and iterative amplitude thresholding," J. Sound Vib. **463**, 114958 (2019).
[8]Y. Ohara, T. Mihara, R. Sasaki, T. Ogata, S. Yamamoto, Y. Kishimoto, and K. Yamanaka, "Imaging of closed cracks using nonlinear response of elastic waves at subharmonic frequency," Appl. Phys. Lett. **90**(1), 011902 (2007).
[9]M. S. Cao, W. Ostachowicz, M. Radzieński, and W. Xu, "Multiscale shear-strain gradient for detecting delamination in composite laminates," Appl. Phys. Lett. **103**(10), 101910 (2013).
[10]I. Solodov, J. Wackerl, K. Pfleiderer, and G. Busse, "Nonlinear self-modulation and subharmonic acoustic spectroscopy for damage detection and location," Appl. Phys. Lett. **84**(26), 5386–5388 (2004).
[11]I. Solodov, J. Bai, and G. Busse, "Resonant ultrasound spectroscopy of defects: Case study of flat-bottomed holes," J. Appl. Phys. **113**(22), 223512 (2013).
[12]I. Solodov, J. Bai, S. Bekgulyan, and G. Busse, "A local defect resonance to enhance acoustic wave-defect interaction in ultrasonic nondestructive evaluation," Appl. Phys. Lett. **99**(21), 211911 (2011).
[13]F. Ciampa, G. Scarselli, and M. Meo, "On the generation of nonlinear damage resonance intermodulation for elastic wave spectroscopy," J. Acoust. Soc. Am. **141**(4), 2364–2374 (2017).
[14]K. Wang, Z. Luo, S. Xu, W. Lai, R. Guan, Q. Liu, M. Liu, J. Rao, and X. Qing, "Analytical insight into local defect resonance induced by disbond in multilayered structures," NDT E Int. **141**, 102976 (2024).
[15]S. Roy and T. Bose, "Efficient determination of local defect resonance frequencies from bicoherence plots using double excitations," Mech. Syst. Sig. Process. **127**, 595–609 (2019).
[16]J. Segers, S. Hedayatrasa, E. Verboven, G. Poelman, W. Van Paepegem, and M. Kersemans, "In-plane local defect resonances for efficient vibrothermography of impacted carbon fiber-reinforced polymers (CFRP)," NDT E Int. **102**, 218–225 (2019).
[17]I. Solodov and M. Kreutzbruck, "Local defect resonance of a through-thickness crack," Ultrasonics **118**, 106565 (2022).
[18]J. Segers, S. Hedayatrasa, G. Poelman, W. Van Paepegem, and M. Kersemans, "Probing the limits of full-field linear local defect resonance identification for deep defect detection," Ultrasonics **105**, 106130 (2020).
[19]Y. Hu, W. Li, C. Zhang, Z. Lan, and M. Deng, "Quantitative assessment of delamination in composites using multiple local-defect-resonance modes," J. Sound Vib. **587**, 118499 (2024).
[20]I. Solodov and G. Busse, "Resonance ultrasonic thermography: Highly efficient contact and air-coupled remote modes," Appl. Phys. Lett. **102**(6), 061905 (2013).
[21]M. S. Cao, H. Xu, R. B. Bai, W. Ostachowicz, M. Radzieński, and L. Chen, "Damage characterization in plates using singularity of scale mode shapes," Appl. Phys. Lett. **106**(12), 121906 (2015).
[22]Z. Lan, O. Saito, and Y. Okabe, "Delamination detection in CFRP laminates using a chirp guided wave mixing technique," NDT E Int. **144**, 103086 (2024).
[23]M. Rahammer, I. Solodov, W. Bisle, D. Scherling, and M. Kreutzbruck, "Thermosonic testing with phase matched guided wave excitation," J. Nondestruct. Eval. **35**(3), 47 (2016).
[24]I. Solodov, A. Dillenz, and M. Kreutzbruck, "A new mode of acoustic NDT via resonant air-coupled emission," J. Appl. Phys. **121**(24), 245101 (2017).
[25]Z. Lan, O. Saito, F. Yu, and Y. Okabe, "Impact damage detection in woven CFRP laminates based on a local defect resonance technique with laser ultrasonics," Mech. Syst. Sig. Process. **207**, 110929 (2024).
[26]J. Hettler, M. Tabatabaeipour, S. Delrue, and K. Van Den Abeele, "Detection and characterization of local defect resonances arising from delaminations and flat bottom holes," J. Nondestruct. Eval. **36**(1), 2 (2017).

[27]D. Dionysopoulos, G.-P. M. Fierro, M. Meo, and F. Ciampa, "Imaging of barely visible impact damage on a composite panel using nonlinear wave modulation thermography," NDT E Int. **95**, 9–16 (2018).
[28]X. Wang, M. Lin, J. Li, J. Tong, X. Huang, L. Liang, Z. Fan, and Y. Liu, "Ultrasonic guided wave imaging with deep learning: Applications in corrosion mapping," Mech. Syst. Sig. Process. **169**, 108761 (2022).
[29]M. Qiu, W. Zheng, J. Chen, Z. Cheng, L. Wang, and Q. Wang, "Highly precise optical positioning through deep learning-assisted photo-thermoelectric detection," Appl. Phys. Lett. **124**(26), 261104 (2024).
[30]X. Li, Y. Wang, X. Liu, Y. Ma, Y. Cai, S. A. Ponomarenko, and X. Liu, "Deep learning and random light structuring ensure robust free-space communications," Appl. Phys. Lett. **124**(21), 214103 (2024).